Research Article | Vol. 25, No. 11 | 29 May 2017 | OPTICS EXPRESS 12357
Optics EXPRESS

Optical pulling and pushing forces exerted on silicon nanospheres with strong coherent interaction between electric and magnetic resonances

HONGFENG LIU, MINGCHENG PANMAI, YUANYUAN PENG, AND SHENG LAN*

Guangdong Provincial Key Laboratory of Nanophotonic Functional Materials and Devices, School of Information and Optoelectronic Science and Engineering, South China Normal University, Guangzhou 510006, China
*slan@scnu.edu.cn

Abstract: We investigated theoretically and numerically the optical pulling and pushing forces acting on silicon (Si) nanospheres (NSs) with strong coherent interaction between electric and magnetic resonances. We examined the optical pulling and pushing forces exerted on Si NSs by two interfering waves and revealed the underlying physical mechanism from the viewpoint of electric- and magnetic-dipole manipulation. As compared with a polystyrene (PS) NS, it was found that the optical pulling force for a Si NS with the same size is enlarged by nearly two orders of magnitude. In addition to the optical pulling force appearing at the long-wavelength side of the magnetic dipole resonance, very large optical pushing force is observed at the magnetic quadrupole resonance. The correlation between the optical pulling/pushing force and the directional scattering characterized by the ratio of the forward to backward scattering was revealed. More interestingly, it was found that the high-order electric and magnetic resonances in large Si NSs play an important role in producing optical pulling force which can be generated by not only *s*-polarized wave but also *p*-polarized one. Our finding indicates that the strong coherent interaction between the electric and magnetic resonances existing in nanoparticles with large refractive indices can be exploited to manipulate the optical force acting on them and the correlation between the optical force and the directional scattering can be used as guidance. The engineering and manipulation of optical forces will find potential applications in the trapping, transport and sorting of nanoparticles.

OCIS codes: (160.4236) Nanomaterials; (160.6000) Semiconductor materials; (290.5850) Scattering, particles; (350.4855) Optical tweezers or optical manipulation.

References and links

1. A. I. Kuznetsov, A. E. Miroshnichenko, Y. H. Fu, J. Zhang, and B. Luk´yanchuk, "Magnetic light," Sci. Rep. **2**, 492 (2012).
2. A. B. Evlyukhin, S. M. Novikov, U. Zywietz, R. L. Eriksen, C. Reinhardt, S. I. Bozhevolnyi, and B. N. Chichkov, "Demonstration of magnetic dipole resonances of dielectric nanospheres in the visible region," Nano Lett. **12**(7), 3749–3755 (2012).
3. L. Shi, T. U. Tuzer, R. Fenollosa, and F. Meseguer, "A new dielectric metamaterial building block with a strong magnetic response in the sub-1.5-micrometer region: silicon colloid nanocavities," Adv. Mater. **24**(44), 5934–5938 (2012).
4. J. M. Geffrin, B. García-Cámara, R. Gómez-Medina, P. Albella, L. S. Froufe-Pérez, C. Eyraud, A. Litman, R. Vaillon, F. González, M. Nieto-Vesperinas, J. J. Sáenz, and F. Moreno, "Magnetic and electric coherence in forward- and back-scattered electromagnetic waves by a single dielectric subwavelength sphere," Nat. Commun. **3**, 1171 (2012).
5. Y. H. Fu, A. I. Kuznetsov, A. E. Miroshnichenko, Y. F. Yu, and B. Luk'yanchuk, "Directional visible light scattering by silicon nanoparticles," Nat. Commun. **4**, 1527 (2013).
6. I. Sinev, I. Iorsh, A. Bogdanov, D. Permyakov, F. Komissarenko, I. Mukhin, A. Samusev, V. Valuckas, A. I. Kuznetsov, B. S. Luk'yanchuk, A. E. Miroshnichenko, and Y. S. Kivshar, "Polarization control over electric and

#291996 https://doi.org/10.1364/OE.25.012357
Journal © 2017 Received 3 Apr 2017; revised 8 May 2017; accepted 9 May 2017; published 17 May 2017

Optics EXPRESS

magnetic dipole resonances of dielectric nanoparticles on metallic films," Laser Photon. Rev. **10**(5), 799–806 (2016).
7. U. Zywietz, C. Reinhardt, A. B. Evlyukhin, T. Birr, and B. N. Chichkov, "Generation and patterning of Si nanoparticles by femtosecond laser pulses," Appl. Phys., A Mater. Sci. Process. **114**(1), 45–50 (2014).
8. U. Zywietz, A. B. Evlyukhin, C. Reinhardt, and B. N. Chichkov, "Laser printing of silicon nanoparticles with resonant optical electric and magnetic responses," Nat. Commun. **5**, 3402 (2014).
9. A. E. Miroshnichenko, A. B. Evlyukhin, Y. F. Yu, R. M. Bakker, A. Chipouline, A. I. Kuznetsov, B. Luk'yanchuk, B. N. Chichkov, and Y. S. Kivshar, "Nonradiating anapole modes in dielectric nanoparticles," Nat. Commun. **6**, 8069 (2015).
10. A. García-Etxarri, R. Gómez-Medina, L. S. Froufe-Pérez, C. López, L. Chantada, F. Scheffold, J. Aizpurua, M. Nieto-Vesperinas, and J. J. Sáenz, "Strong magnetic response of submicron silicon particles in the infrared," Opt. Express **19**(6), 4815–4826 (2011).
11. A. B. Evlyukhin, C. Reinhardt, A. Seidel, B. S. Luk'yanchuk, and B. N. Chichkov, "Optical response features of Si-nanoparticle arrays," Phys. Rev. B **82**(4), 045404 (2010).
12. A. I. Kuznetsov, A. E. Miroshnichenko, M. L. Brongersma, Y. S. Kivshar, and B. Luk'yanchuk, "Optically resonant dielectric nanostructures," Science **354**(6314), 2472 (2016).
13. S. Person, M. Jain, Z. Lapin, J. J. Sáenz, G. Wicks, and L. Novotny, "Demonstration of zero optical backscattering from single nanoparticles," Nano Lett. **13**(4), 1806–1809 (2013).
14. M. Kerker, D. S. Wang, and C. L. Giles, "Electromagnetic scattering by magnetic spheres," J. Opt. Soc. Am. **73**(6), 765–767 (1983).
15. J. Yan, P. Liu, Z. Lin, H. Wang, H. Chen, C. Wang, and G. Yang, "Directional Fano resonance in a silicon nanosphere dimer," ACS Nano **9**(3), 2968–2980 (2015).
16. Y. Tsuchimoto, T. A. Yano, T. Hayashi, and M. Hara, "Fano resonant all-dielectric core/shell nanoparticles with ultrahigh scattering directionality in the visible region," Opt. Express **24**(13), 14451–14462 (2016).
17. D. S. Filonov, A. P. Slobozhanyuk, A. E. Krasnok, P. A. Belov, E. A. Nenasheva, B. Hopkins, A. E. Miroshnichenko, and Y. S. Kivshar, "Near-field mapping of Fano resonances in all-dielectric oligomers," Appl. Phys. Lett. **104**(2), 021104 (2014).
18. A. E. Miroshnichenko and Y. S. Kivshar, "Fano resonances in all-dielectric oligomers," Nano Lett. **12**(12), 6459–6463 (2012).
19. B. Hopkins, A. N. Poddubny, A. E. Miroshnichenko, and Y. S. Kivshar, "Revisiting the physics of Fano resonances for nanoparticle oligomers," Phys. Rev. A **88**(5), 053819 (2013).
20. P. Albella, M. A. Poyli, M. K. Schmidt, S. A. Maier, F. Moreno, J. J. Sáenz, and J. Aizpurua, "Low-loss electric and magnetic field-enhanced spectroscopy with subwavelength silicon dimers," J. Phys. Chem. C **117**(26), 13573–13584 (2013).
21. H. Wang, P. Liu, Y. Ke, Y. Su, L. Zhang, N. Xu, S. Deng, and H. Chen, "Janus magneto-electric nanosphere dimers exhibiting unidirectional visible light scattering and strong electromagnetic field enhancement," ACS Nano **9**(1), 436–448 (2015).
22. A. Ashkin, "Acceleration and trapping of particles by radiation pressure," Phys. Rev. Lett. **24**(4), 156–159 (1970).
23. A. Ashkin, J. M. Dziedzic, J. E. Bjorkholm, and S. Chu, "Observation of a single-beam gradient force optical trap for dielectric particles," Opt. Lett. **11**(5), 288 (1986).
24. O. Brzobohatý, M. Šiler, J. Trojek, L. Chvátal, V. Karásek, A. Paták, Z. Pokorná, F. Mika, and P. Zemánek, "Three-dimensional optical trapping of a plasmonic nanoparticle using low numerical aperture optical tweezers," Sci. Rep. **5**(1), 8106 (2015).
25. O. Brzobohatý, M. Šiler, L. Chvátal, V. Karásek, and P. Zemánek, "Optical trapping of non-spherical plasmonic nanoparticles," Proc. SPIE **8999**, 899909 (2014).
26. P. Jákl, A. V. Arzola, M. Šiler, L. Chvátal, K. Volke-Sepúlveda, and P. Zemánek, "Optical sorting of nonspherical and living microobjects in moving interference structures," Opt. Express **22**(24), 29746–29760 (2014).
27. O. Brzobohatý, M. Šiler, J. Ježek, P. Jákl, and P. Zemánek, "Optical manipulation of aerosol droplets using a holographic dual and single beam trap," Opt. Lett. **38**(22), 4601–4604 (2013).
28. S. Kawata and T. Sugiura, "Movement of micrometer-sized particles in the evanescent field of a laser beam," Opt. Lett. **17**(11), 772–774 (1992).
29. G. Volpe, R. Quidant, G. Badenes, and D. Petrov, "Surface plasmon radiation forces," Phys. Rev. Lett. **96**(23), 238101 (2006).
30. C. Min, Z. Shen, J. Shen, Y. Zhang, H. Fang, G. Yuan, L. Du, S. Zhu, T. Lei, and X. Yuan, "Focused plasmonic trapping of metallic particles," Nat. Commun. **4**, 2891 (2013).
31. P. P. Patra, R. Chikkaraddy, R. P. Tripathi, A. Dasgupta, and G. V. Kumar, "Plasmofluidic single-molecule surface-enhanced Raman scattering from dynamic assembly of plasmonic nanoparticles," Nat. Commun. **5**, 4357 (2014).
32. M. L. Juan, M. Righini, and R. Quidant, "Plasmon nano-optical tweezers," Nat. Photonics **5**(6), 349–356 (2011).
33. A. Andres-Arroyo, B. Gupta, F. Wang, J. J. Gooding, and P. J. Reece, "Optical manipulation and spectroscopy of silicon nanoparticles exhibiting dielectric resonances," Nano Lett. **16**(3), 1903–1910 (2016).
34. J. Chen, J. Ng, K. Ding, K. H. Fung, Z. Lin, and C. T. Chan, "Negative optical torque," Sci. Rep. **4**(1), 6386 (2015).

Optics EXPRESS

35. J. Chen, N. Wang, L. Cui, X. Li, Z. Lin, and J. Ng, "Optical twist induced by plasmonic resonance," Sci. Rep. **6**(1), 27927 (2016).
36. J. Chen, J. Ng, Z. F. Lin, and C. T. Chan, "Optical pulling force," Nat. Photonics **5**(9), 531–534 (2011).
37. O. Brzobohatý, V. Karásek, M. Šiler, L. Chvátal, T. Čižmár, and P. Zemánek, "Experimental demonstration of optical transport, sorting and self-arrangement using a 'tractor beam'," Nat. Photonics **7**(2), 123–127 (2013).
38. S. Sukhov and A. Dogariu, "Negative nonconservative forces: optical "tractor beams" for arbitrary objects," Phys. Rev. Lett. **107**(20), 203602 (2011).
39. A. Novitsky, C. W. Qiu, and H. Wang, "Single gradientless light beam drags particles as tractor beams," Phys. Rev. Lett. **107**(20), 203601 (2011).
40. S. H. Lee, Y. Roichman, and D. G. Grier, "Optical solenoid beams," Opt. Express **18**(7), 6988–6993 (2010).
41. R. Gómez-Medina, B. García-Cámara, I. Suárez-Lacalle, F. González, F. Moreno, M. Nieto-Vesperinas, and J. J. Sáenz, "Electric and magnetic dipolar response of germanium nanospheres: interference effects, scattering anisotropy, and optical forces," J. Nanophotonics **5**(1), 053512 (2011).
42. A commercial software developed by Lumerical Solutions Inc. (https://www.lumerical.com) is used for the numerical simulations.
43. M. Nieto-Vesperinas, J. J. Sáenz, R. Gómez-Medina, and L. Chantada, "Optical forces on small magnetodielectric particles," Opt. Express **18**(11), 11428–11443 (2010).
44. J. R. Arias-González and M. Nieto-Vesperinas, "Optical forces on small particles: attractive and repulsive nature and plasmon-resonance conditions," J. Opt. Soc. Am. A **20**(7), 1201–1209 (2003).
45. M. Nieto-Vesperinas, R. Gomez-Medina, and J. J. Sáenz, "Angle-suppressed scattering and optical forces on submicrometer dielectric particles," J. Opt. Soc. Am. A **28**(1), 54–60 (2011).
46. P. C. Chaumet and A. Rahmani, "Electromagnetic force and torque on magnetic and negative-index scatterers," Opt. Express **17**(4), 2224–2234 (2009).
47. P. C. Chaumet and M. Nieto-Vesperinas, "Time-averaged total force on a dipolar sphere in an electromagnetic field," Opt. Lett. **25**(15), 1065–1067 (2000).
48. C. F. Bohren and D. R. Huffman, *Absorption and Scattering of Light by Small Particles* (John Wiley & Sons, 1983).

1. Introduction

In recent years, silicon (Si) nanospheres (NSs) with diameters ranging from 100 to 250 nm, which exhibit distinct electric and magnetic dipole (ED and MD) resonances in the visible to near inferred spectral range, have attracted tremendous interest because they are considered as the most promising building blocks for metamaterials operating at optical frequencies where artificial atoms made of metals fail to work due to large Ohmic loss [1–13]. One remarkable feature of such Si NSs is the MD induced by a circular displacement current which results in the strong scattering of white light termed as "magnetic light" [1]. Directional scattering of such Si NSs has been studied in both the microwave and the visible to near infrared spectral ranges and it was found that Si NSs exhibit much different forward and backward scattering at specific wavelengths [4,5] (e.g., the wavelengths satisfying the first and second Kerker conditions [14]).

Very recently, Fano resonances were observed in Si NS dimers and core-shell Si NSs [15,16], which belong to all-dielectric systems, and they were attributed to the interference between the significantly broadened EDs and the nearly unbroadened MDs of the coupled Si NSs or core-shell Si NSs. In these cases, the Fano resonances were observed near the wavelengths of the MDs. In fact, Fano resonances were also observed in the oligomer of Si or Au NSs owing to the collective interaction between the constituent Si or Au NSs [17–21]. In general, the directional scattering and Fano resonances indicate the existence of strong coherent interaction between the EDs and MDs in Si NSs. From the viewpoint of momentum conservation, the large forward scattering implies a weak optical force in the forward direction while a large backward scattering indicates a strong optical force in the forward direction.

In the field of optical trapping, Ashkin *et al.* discovered the existence of radiation pressure in 1970s and demonstrated a technique now referred to as optical tweezers in 1980s [22,23]. Since then, optical trapping have attracted tremendous interest in both fundamental research and device application [24–27]. In conventional optical tweezers, the balance between gradient force and scattering force is exploited to capture particles. Various methods have been proposed to realize the trapping of micro- and nanoparticles, such as the use of

Optics EXPRESS

evanescent field [28] and surface plasmons [29–32]. Si nanoparticles have already been experimentally trapped in an optical tweezers [33]. The investigation of optical torque based on optical force was also carried out [34,35]. In recent years, optical pulling force, which makes particles move against the propagation direction of light in the absence of intensity gradient, has stimulated the interest of researchers working in this field because it is a counter-intuitive phenomenon since the discovery of optical radiation pressure. It was discussed theoretically by Chen *et al.* by using a Bessel beam and demonstrated experimentally by Brzobohatý *et al.* by using two interfering waves [36,37]. Several scenarios have been proposed to achieve optical pulling force [38–40]. Although the optical beams used in the analytical model or the configurations used in the experimental demonstration are different, the underlying physical mechanism for optical pulling force is the strong scattering of the incident light in the forward direction which leads to an optical force against the photon stream based on the conservation of momentum.

So far, the particles used in the study of optical pulling force are polystyrene (PS) beads with relative large radius. For trapping light with a wavelength of 1064 nm, it was found that optical pulling force occurs only for PS beads with radius larger than 400 nm [36]. For nanoparticles with large refractive indices such as Si, germanium (Ge) and gallium arsenide (GaAs) NSs, it is expected that optical pulling force can be achieved at a much smaller size because of the significant directional scattering resulted from the strong coherent interaction between EDs and MDs. The optical force generated by single plane wave irradiation has been systematically investigated for Ge NSs [41]. In this case, the total optical force (F_{total}) can be decomposed into three components of F_e, F_m, and F_{em} which are related to the ED, MD and their coherent interaction, respectively. It was revealed that F_e and F_m are positive while F_{em} is negative. In the case of single plane wave irradiation, however, F_{em} cannot beat F_e and F_m and the total optical force ($F_{total} = F_e + F_m + F_{em}$) is always positive. It implies that optical pulling force cannot be generated by using single plane wave irradiation. Such a conclusion is obvious from the momentum conservation theory. In the limit case of all the incident photons are scattered in the forward direction, one can only expect a zero optical force. If we consider two interfering waves, then it is possible to generate optical pulling force for Si NSs with small sizes which will be interesting for the researchers in the fields of both all-dielectric metamaterials and optical trapping. In other words, the two hot topics belonging to different research fields (i.e. all-dielectric metamaterials and optical forces) are bridged by the strong directional scattering which has been observed for Si NSs. Therefore, it seems very interesting to investigate not only the optical pulling force but also the optical pushing force for Si NSs. In Fig. 1, we show schematically the Si NS irradiated by two interfering waves with *s*- and *p*-polarizations considered in this work. The orientations of the ED and MD induced by the two interfering waves with different polarizations and the resulting directional scattering and optical force are also illustrated.

2. Theoretical and numerical methods

The scattering spectra described in this work were either calculated by using Mie theory (see Appendix Information, Section 6.1) or simulated by using the finite-difference time-domain (FDTD) technique [42]. The nanoparticles discussed in this paper, including Si and PS NSs, are assumed to be immersed in water with a refractive index of 1.33. The optical forces acting on Si NSs were either theoretically calculated based on the Maxwell strain tensor or numerically simulated based on the FDTD method. In the FDTD simulation, the volumetric technique analysis group was used to calculate the optical force acting on Si and PS NSs. The calculated optical force has been normalized to the power of the incident light. In the numerical simulations, a non-uniform grid with the smallest size of 1 nm as well as a perfectly matched boundary condition was employed. A detailed description of the theoretical method used to calculate the optical force is provided in Appendix Information (see Section 6.2).

Optics EXPRESS

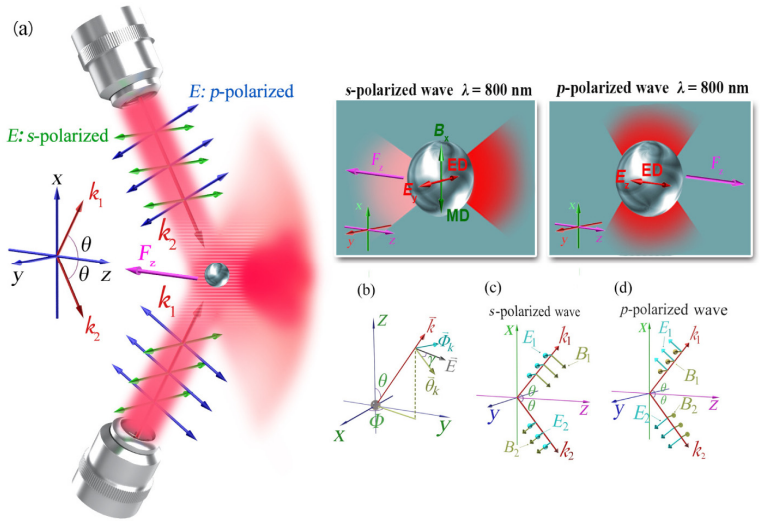

Fig. 1. (a) Schematic showing the use of two interfering waves to generate an optical pulling force for a Si NS. The orientations of the ED and MD induced in the Si NS by the two interfering waves with *s*- and *p* polarizations and the resulting directional scattering and optical force are illustrated. (b) Various parameters used to characterize the incident plane wave. (c) and (d) Schematics showing two *s*- and *p*-polarized waves, respectively.

3. Results and discussion

3.1 Physical origin of the optical pulling force

For Si NSs with diameters ranging from 100 to 250 nm, one can see well-defined EDs and MDs appearing in the visible to near infrared spectral range. If the light wavelength is chosen in this spectral range, it is generally sufficient to consider only the EDs and MDs with coherent interaction when discussing the optical force acting on such Si NSs. In this case, we consider a Si NS as a dipolar particle embedded in a medium with relative dielectric permittivity ε and magnetic permeability μ, irradiated by an incident light whose electric and magnetic fields are $E^{(i)}$ and $B^{(i)}$, respectively. In the dipolar approximation, the scattered field of the Si NS corresponds to that radiated by the induced electric and magnetic dipole moments, $\boldsymbol{p}$ and $\boldsymbol{m}$, respectively. The total time-averaged optical force acting on the Si NS can be expressed as [43–45]:

$$\left\langle \vec{F} \right\rangle = \frac{1}{2}\Re\left[\left(\nabla \otimes \vec{E}^{(i)*} \right) \cdot \vec{p} + \left(\nabla \otimes \vec{B}^{(i)*} \right) \cdot \vec{m} - \frac{2k^4}{3}\sqrt{\frac{\mu}{\varepsilon}} \left(\vec{p} \times \vec{m}^* \right) \right] \qquad (1)$$

Eq. (1) represents the generalized result for the time-averaged optical force acting on the Si NS immersed in a medium with refractive index of $n = \sqrt{\varepsilon\mu}$ [46]. The wavenumber is $k = n\omega/c$, ω being the frequency. The symbol $\otimes$ represents the dyadic product so that the matrix operation $\left(\nabla \otimes \vec{V} \right) \cdot \vec{W}$ has elements $W_j \partial_i V_j$ for $i, j = 1, 2, 3$. The first two terms in Eq. (1) are the optical force exerted by the incident light on the induced electric and magnetic dipoles (i.e., $\langle F_e \rangle$ and $\langle F_m \rangle$) while the third term is the optical force originating from the interaction between the two dipoles (i.e., $\langle F_{em} \rangle$) [46,47].

Previously, the optical force exerted on a Si or Ge NS which is irradiated by a single plane wave has been discussed and the contributions of the ED, MD and their coherent interaction to the optical force (i.e., F_e, F_m, and F_{em}) has been clarified [41,45]. Although F_{em} can be negative at some wavelengths, optical pulling force cannot be realized in the case of single plane wave irradiation. Now we can theoretically analyze the optical force exerted on

Optics EXPRESS

the Si NS by two interfering waves. The electric field created by the two interfering waves with an incidence angle of θ [see the definition in Fig. 1(a)] can be expressed as follows:

$$\vec{E} = E_0 \sum_{i=1,2} \left(\vec{\theta}_{ki} \cos\gamma_i + \vec{\phi}_{ki} \sin\gamma_i \right) \exp\left(ik\vec{k}_i \cdot \vec{r} \right), \tag{2}$$

where $\vec{k}_i = \left(\sin\theta_{ki} \cos\phi_{ki}, \sin\theta_{ki} \sin\phi_{ki}, \cos\theta_{ki} \right)$, $\vec{\theta}_{ki} = \left(\cos\theta_{ki} \cos\phi_{ki}, \cos\theta_{ki} \sin\phi_{ki}, -\sin\theta_{ki} \right)$, and $\vec{\phi}_{ki} = \vec{k}_i \times \vec{\theta}_{ki}$ [see Fig. 1(b) for the definitions of γ and ϕ].

For *s*-polarized wave, we have $\gamma_1 = \pi/2, \theta_{k1} = \theta, \phi_{k1} = 0$, $\gamma_2 = 3\pi/2, \theta_{k2} = \theta, \phi_{k2} = \pi$. In this case, the optical force in the z direction (F_z), which can be derived by substituting the above parameters into Eqs. (2) and (1) (see Appendix Information), is expressed as:

$$\begin{aligned} \left\langle \vec{F} \right\rangle_z^s &= \left\langle \vec{F}_{\mathrm{e}} \right\rangle_z^s + \left\langle \vec{F}_m \right\rangle_z^s + \left\langle \vec{F}_{em} \right\rangle_z^s \\ &= 4F_0 \left[\frac{1}{r^3} \Im\left(\varepsilon^{-1} \alpha_e \cos\theta + \mu \alpha_m \cos^3\theta \right) - \frac{2\mu k^3}{3\varepsilon r^3} \Re\left(\alpha_e \alpha_m^* \right) \cos\theta \right], \end{aligned} \tag{3}$$

where $F_0 = \varepsilon r^3 k E_0^2 / 2$, α_{e} and α_{m} are the electric and magnetic polarizabilities of the Si NS which can be determined by the Mie coefficients (see Appendix), $\Im$ and $\Re$ stand for the imaginary and real parts of a complex. In Fig. 1, it can be seen that the *z* components of the wavevectors of the two incident waves are in the + *z* direction. For this reason, the optical forces in the + *z* and –*z* directions are referred to as optical pushing and pulling forces, respectively.

By comparing Eq. (3) with Eq. (13) in [41], it can be easily found that a factor of $4\cos\theta$ is added in F_{e} and F_{em} while a factor of $4\cos^3\theta$ is included in F_{m} when the illumination source is changed from single plane wave to two interfering waves. For this reason, it is expected that F_{e} and F_{em} decrease in a slower rate ($\cos\theta$) as compared with F_m ($\cos^3\theta$) when the incidence angle is increased. As a result, F_{em} may exceed the sum of F_{m} and F_{e} and become dominant after a critical value of θ. In this case, a negative force (i.e., pulling force) is created by the two interfering waves.

From the viewpoint of momentum conservation, it is impossible to generate optical pulling force by using single plane wave irradiation because the momentum of the photons being scattered into the forward direction cannot exceed the initial momentum of the incident photons. However, the generation of optical pulling force becomes possible when two interfering waves are employed. If the most of the incident photons are scattered into the forward direction, then the momentum of the scattered photons may become larger than the sum of the momentums of the two incident waves along this direction when the angle between them exceeds a critical value. In this case, an optical pulling force is generated. Therefore, the generation of optical pulling force is closely related to the directional scattering of nanoparticles. It has been demonstrated that Si NSs exhibit directional scattering in the visible and near infrared spectral range. Thus, optical pulling force is expected to occur at the wavelength where the maximum ratio of forward to backward scattering is achieved.

In Fig. 2(a), we present the spectrum of the total optical force $F_{\mathrm{total}}(\lambda)$ acting on a Si NS with a radius of r = 100 nm calculated by using Eq. (13) in [41]. It appears to be quite similar to the scattering spectrum of the Si NS. If we decompose the spectrum into the contributions of $F_{\mathrm{e}}(\lambda)$, $F_{\mathrm{m}}(\lambda)$ and $F_{\mathrm{em}}(\lambda)$, it can be seen that $F_{\mathrm{e}}(\lambda)$ and $F_{\mathrm{m}}(\lambda)$ look like very much the Mie scattering coefficients $a_1(\lambda)$ and $b_1(\lambda)$ which represent the contributions of the ED and MD to the total scattering. Apparently, $F_{\mathrm{e}}(\lambda)$ and $F_{\mathrm{m}}(\lambda)$ remain to be positive over the entire spectral range. In sharp contrast, $F_{\mathrm{em}}(\lambda)$ appears to be negative and reaches a minimum value on the right side of the MD. Since $F_{\mathrm{em}}(\lambda)$ cannot counteract $F_{\mathrm{e}}(\lambda)$ and $F_{\mathrm{m}}(\lambda)$, $F_{\mathrm{total}}(\lambda)$ remains to be positive over the entire spectral range and no optical pulling force can be realized by using

Optics EXPRESS

single plane wave irradiation, as discussed above. In Fig. 2(b), we show the spectra of $F_{total}(\lambda)$ and its constituents [$F_e(\lambda)$, $F_m(\lambda)$ and $F_{em}(\lambda)$] when the Si NS is irradiated with two interfering waves. In this case, the two interfering waves are assumed to be *s*-polarized with an incidence angle of $\theta = 78°$. It is noticed that $F_e(\lambda)$ and $F_{em}(\lambda)$ remain nearly unchanged while a significant reduction of $F_m(\lambda)$ to nearly zero is observed. As a result, optical pulling force can be achieved in a narrow wavelength range of 780–830 nm. As will be shown later, the optical pulling force is reduced rapidly if the polarization angle of the incident wave is varied from 90° (*s*-polarized) to 0° (*p*-polarized).

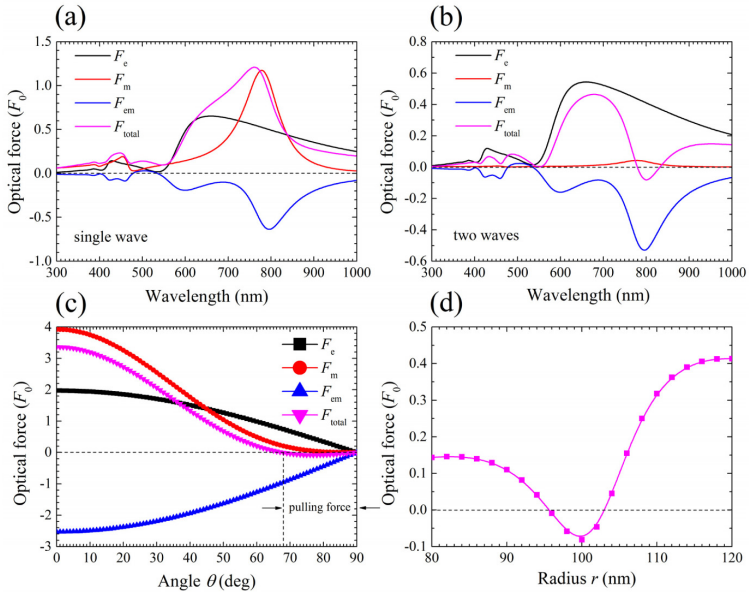

Fig. 2. Wavelength dependence of the total optical force (F_{total}) and various components (F_e, F_m, and F_{em}) acting on the Si NS with $r = 100$ nm calculated for the irradiation of single plane wave (a) and two *s*-polarized waves with an incidence angle of $\theta = 78°$ (b). (c) Dependence of total optical force (F_{total}) and various components (F_e, F_m, and F_{em}) on the incidence angle. (d) Dependence of the optical force in the *z* direction (F_z) on the radius of the Si NS calculated for two *s*-polarized waves with $\lambda = 800$ nm and $\theta = 78°$.

Physically, the configuration of two-wave irradiation offers us the opportunity to manipulate the spatial orientations of the ED and MD excited in the Si NS and thus the directional scattering of the Si NS. For *p*-polarized wave, the MDs induced by the two incident waves are canceled out because they are antiparallel and in phase, as shown in Figs. 1(a) and 1(d). As a result, $F_m(\lambda)$ and $F_{em}(\lambda)$ disappear completely whereas $F_e(\lambda)$ remains to be a positive value. Therefore, no optical pulling force will be generated if only the ED and MD of the Si NS are considered [see Appendix Information, Eq. (19)-Eq. (23)]. For *s*-polarized wave, the electric field does not change with the incidence angle because it is in the *y* direction (i.e., $E_y = E_0$). On the other hand, the *z* components of the magnetic field of the two incident waves are canceled out because they are antiparallel and in phase. A constructive enhancement is expected for the *x* components of the magnetic field of the two incident waves, as shown in Figs. 1(a) and 1(c). In this case, the magnetic field is in the *x* direction and the induced magnetic dipole decreases with increasing incidence angle ($B_x = B\cos\theta$). As a result, $F_m(\lambda)$ decreases more rapidly than $F_{em}(\lambda)$ and optical pulling force is available for incidence angles larger than a critical value [see Appendix Information, Eq. (12)–Eq. (15)].

Theoretically, we have calculated the dependence of F_e, F_m, F_{em}, and F_{total} at $\lambda = 800$ nm on the incidence angle (θ), as shown in Fig. 2(c). While the dependence of F_e and F_{em} on θ follows a function of $\cos\theta$, the dependence of F_m on θ follows a function of $\cos^3\theta$. It means

Optics EXPRESS

that F_m decreases more rapidly than F_e and F_{em} with increasing θ. As a result, there exists an angle range ($68° \leq \theta \leq 90°$) in which F_{em} beats F_e and F_m, leading to the generation of optical pulling force. By fixing the light wavelength at λ = 800 nm and the incidence angle at θ = 78°, we also examined the dependence of the optical pulling force (F_z) on the size of the Si NS, as shown in Fig. 2(d). It can be seen that the maximum optical pulling force is achieved in the Si NS with r = 100 nm.

3.2 Strong optical pulling force observed in Si NSs

Previously, Chen *et al.* studied theoretically the optical pulling force acting on PS NSs with different sizes by using two interfering beams at 1064 nm with θ = 87° [36]. However, the influence of the polarization, wavelength and incident angle on the optical pulling force has not been discussed in detail. Zemanek *et al.* also studied theoretically the optical pulling force acting on a PS NS with r = 410 nm by using two interfering light at 532 nm. They found that optical pulling force couldn't be generated by *p*-polarized light. For *s*-polarized light, the optical pulling force was observed only for a narrow incidence angle range of $79° \leq \theta \leq 90°$, where θ is the half angle between the two interfering light which is the same as that defined in Fig. 1. As discussed above, the coherent interaction between the ED and MD is expected to be much stronger in Si NSs than that in PS NSs. As a result, directional scattering appears to be more significant in Si NSs than that in PS NSs.

Here, we investigated theoretically the optical force exerted on a Si NS with r = 100 nm by two interfering light at 800 nm. In order to see the effects of light polarization on the optical pulling force, the z component of the total optical force (F_z) as a function of θ has been calculated for incident light with different polarization angles of γ = 0°, 30°, 60°, and 90°, as shown in Fig. 3(a). Here, polarization angles of 0° and 90° correspond to *p*- and *s*-polarized light, respectively. Although optical pulling force is still not available for *p*-polarized light, it can be seen that optical pulling force can be obtained in a much wider angle range of $68° \leq \theta \leq 90°$ for *s*-polarized light, as shown in Fig. 3(a). In addition, the maximum optical pulling force is achieved at θ = 78°. Obviously, the wider angle range achieved in Si NSs makes it easier to experimentally investigate optical pulling force. For comparison, we calculated the dependence of optical force acting on Si and PS NSs with the same radius of r = 100 nm on the incidence angle for *p*- and *s*-polarized light, as shown in Fig. 3(b). Apart from the wide angle range observed for the Si NS, it can be seen that the optical pulling force acting on the Si NS is enhanced by a factor of ~70 as compared with the PS NS. Such an enhancement arises from the strong coherent interaction between the ED and MD in the Si NS which leads to the stronger scattering in the forward direction. In order to see the correlation between the optical pulling force and the directional scattering, we have calculated the radiation patterns of the Si NS in the xz plane for the incident waves with different polarization angles, as shown in Fig. 3(c). For γ = 90° (*s*-polarized), it can be seen that the forward scattering is much stronger than the backward one and a large optical pulling force is obtained. For γ = 60°, the forward scattering remains much stronger than the backward one. However, the optical pulling force is reduced significantly. The reduction of the optical pulling force is caused mainly by the reduction of the induced magnetic dipole. As γ is reduced to 30°, no optical pulling force is available although the forward scattering is still stronger than the backward one because the net momentum of the forward scattering cannot exceed the initial momentum of the incident photons in the z-direction. For γ = 0° (*p*-polarized), only the ED along the z direction is induced in the Si NS and the radiation pattern appears as the typical one for a dipole.

Optics EXPRESS

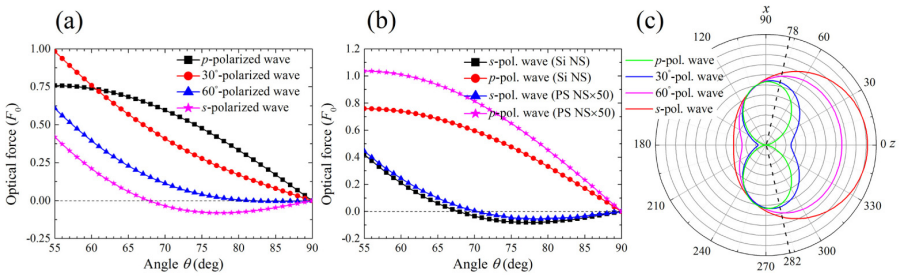

Fig. 3. (a) Dependence of the optical force in the z direction exerted on the Si NS with r = 100 nm on the incidence angle calculated for the incident wave with polarization angles of γ = 0° (p-polarized), 30°, 60°, and 90° (s-polarized). (b) Dependence of the optical force in the z direction on the incidence angle calculated for the Si and PS NSs with r = 100 nm irradiated with s- and p-polarized waves. In both cases, the wavelength of the incident wave is chosen at the minimum of F_{em} (λ = 800 nm for the Si NS and λ = 340 nm for the PS NS). (c) Radiation patterns of the Si NS with r = 100 nm in the xz plane calculated at λ = 800 nm for γ = 0° (p-polarized), 30°, 60°, and 90° (s-polarized) with an incidence angle of θ = 78°.

3.3 Strong optical pushing force observed at magnetic quadrupole resonance

By using the formula presented in Section 3.1, one can easily calculate the optical force acting on a nanoparticle which can be described approximately by an ED and a MD. In other words, only the ED and MD induced by the incident wave are taken into account in the simple theoretical model. The advantage of the theoretical analysis is the decomposition of the total optical force into the contributions of the ED, MD and their coherent interaction. For nanoparticles with large sizes, however, one need to consider the contributions of high-order electric and magnetic resonances and the addition of such high-order resonances makes the theoretical calculation of optical force more complicate. In this case, numerical simulation based on the FDTD method appears to be a more convenient way to analyze the optical force acting on nanoparticles.

In Fig. 4(a), we present the wavelength dependence of the optical force (pulling or pushing) in the z direction (F_z) for a Si NS with r = 100 nm and θ = 78° simulated by using the FDTD method. The same optical force calculated by using the theoretical model considering only the ED and MD is also provided for comparison. It can be seen that the optical force calculated by using the two methods agree well for wavelengths longer than 600 nm. In means that the consideration of only the ED and MD of the Si NS in the calculation of the optical force is sufficient if the wavelength of the incident wave is chosen to be larger than 600 nm. In Fig. 4(b), we compare the wavelength dependence of the optical force in the z direction and the scattering spectrum of the Si NS and identify three remarkable features. First, the maximum optical pulling force is achieved at the long-wavelength side of the MD. Second, the optical force disappears completely at the MD of the Si NS. Finally, it is noticed that an optical pushing force as large as ~4.5 pN is achieved at the magnetic quadrupole (MQ) resonance. Since the MQ resonance is quite sensitive to the size of the Si NS, the strong optical pushing force appearing at the MQ may be exploited in the sorting of nanoparticles. In Fig. 4(b), we also present the absorption spectrum of the Si NS. It can be seen that the absorption at the MD and ED of the Si NS is negligible while a maximum absorption is observed at the MQ. The reasons for this phenomenon are twofold. First, the imaginary part of the complex refractive index of Si increases rapidly for wavelengths shorter than 600 nm. Second, very large electric field enhancement is observed at the MQ. These two factors lead to the strong absorption observed at the MQ. From the viewpoint of momentum conservation, the large absorption at the MQ also contributes the optical force in the forward direction.

Optics EXPRESS

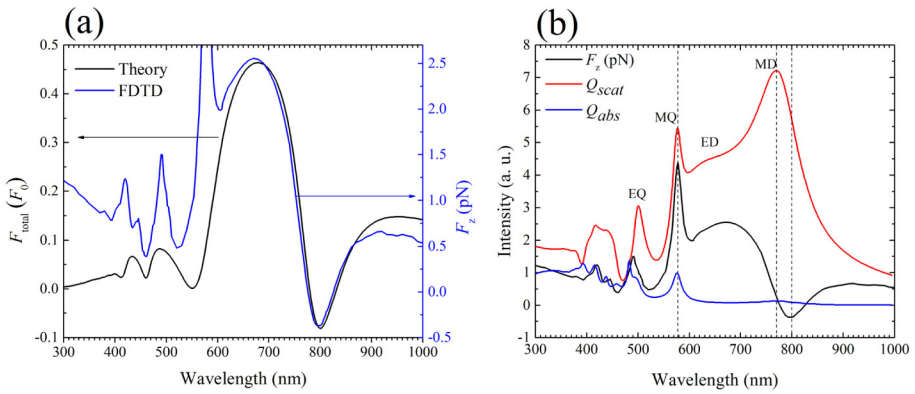

Fig. 4. (a) Wavelength dependence of the optical force in the z direction calculated theoretically and simulated numerically for the s-polarized wave with $\theta = 78°$. (b) Comparison of the spectrum of the optical force in the z direction with the scattering spectrum of the Si NS with $r = 100$ nm. The absorption spectrum of the Si NS is also provided.

3.4 Correlation between optical pulling/pushing force and directional scattering

In Fig. 5, we show the wavelength dependence of the ratio of the forward to backward scattering and compare it with the wavelength dependence of the optical force in the z direction. It can be seen that the largest optical pulling force is achieved at the wavelength where the largest ratio of the forward to backward scattering is observed (λ ~800 nm). In addition, the strongest optical pushing force is obtained at the MQ where the minimum ratio of the forward to backward scattering is observed (λ ~580 nm).

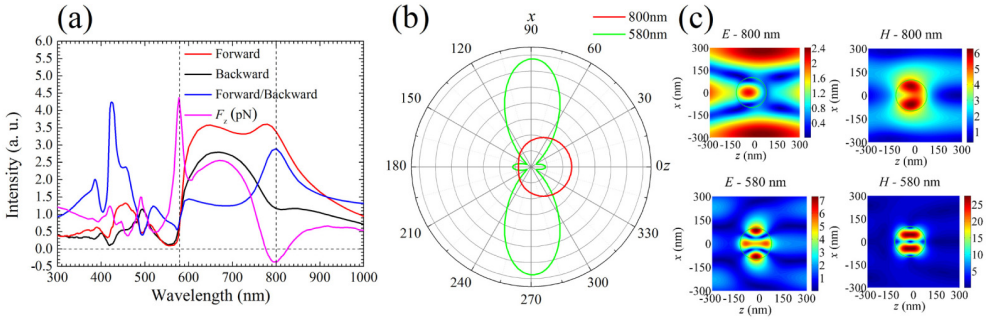

Fig. 5. (a) Correlation between the spectrum of the optical force and that of the ratio of the forward to backward scattering. (b) Radiation patterns in the xz plane calculated at $\lambda = 800$ and 580 nm for two s-polarized waves with $\theta = 78°$. (c) Electric and magnetic field distributions calculated for the Si NS with $r = 100$ nm at $\lambda = 800$ and 580 nm where the maximum optical pulling and pushing forces are observed, respectively.

It should be emphasized that the maximum ratio of the forward to backward scattering is only the necessary condition for the achievement of optical pulling force, not the sufficient condition. For example, the backward scattering vanishes at the wavelength where the first Kerker condition [14] is satisfied and the ratio of the forward to backward scattering is infinite in the case of single plane wave irradiation. However, no optical pulling force is generated at this wavelength. In order to gain a deep insight into the correlation between the optical pulling/pushing force and the directional scattering, we also calculated the radiation patterns of the Si NS at 800 and 580 nm, as shown in Fig. 5(b). For the incident light with λ = 800 nm, it can be seen that the forward scattering is about 3 times stronger than the backward one. In contrast, the scattering occurs mainly in the x direction for the incident light with λ = 580 nm. The scattering intensity in the z direction is quite weak. In this case, it is noticed that

Optics EXPRESS

the forward scattering is weaker than the backward one. In Fig. 5(c), we present the electric and magnetic field distributions for the Si NS calculated at λ = 800 and 580 nm where the maximum optical pulling and pushing forces are achieved, respectively.

3.5 Optical pulling force utilizing the high-order electric and magnetic resonances

Now we fix λ = 800 nm and θ = 85° and examine the dependence of the optical force in the z direction on the radius of the Si NS, as shown in Fig. 6(a). It can be seen that very large optical pulling force can be achieved for Si NSs with r ~450 nm. More interestingly, optical pulling force is available not only for s-polarized wave but also for p-polarized one. In addition, the optical pulling force generated by p-polarized wave reaches half of that generated by s-polarized wave.

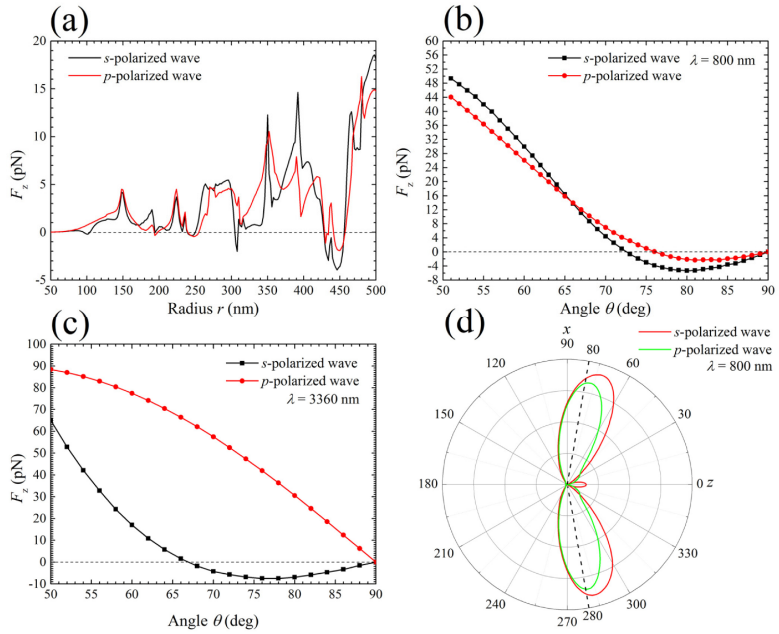

Fig. 6. (a) Dependence of the optical force in the z direction on the radius of the Si NS calculated for s- and p-polarized waves with λ = 800 nm and θ = 85°. (b) Dependence of the optical force in the z direction acting on a Si NS with r = 450 nm on the incidence angle calculated for s- and p-polarized waves at λ = 800 nm. (c) Dependence of the optical force in the z direction acting on a Si NS with r = 450 nm on the incidence angle calculated for s- and p-polarized waves at λ = 3360 nm. (d) Radiation patterns of the Si NS with r = 450 nm calculated for s- and p-polarized waves with λ = 800 nm and θ = 80°.

In order to gain a deep insight into these phenomena, we calculated the dependence of the optical force on the incidence angle for both s- and p-polarized waves, as shown in Fig. 6(b). It can be seen that the maximum optical pulling force as large as ~6 pN is obtained at θ ~80° for s-polarized wave. For p-polarized wave, the maximum optical pulling force of ~3 pN is achieved at a larger angle of θ ~84°. Actually, the largest optical force for the Si NS with r = 450 nm is obtained at λ = 3360 nm where the maximum F_{em} is observed, as shown in Fig. 6(c). In this case, the optical pulling force is calculated to be ~8 pN for s-polarized wave but it is not available for p-polarized wave. From the experimental point of view, however, the use of 800-nm laser light is more attractive because the optical pulling force can be achieved not only for s-polarized light but also for p-polarized light. It means that the high-order electric and magnetic resonances of large Si nanoparticles can be exploited to realize optical pulling force. In Fig. 6(d), we show the radiation patterns of the Si NS with r = 450 nm calculated for s- and p-polarized waves at λ = 800 nm. It can be seen that the radiation

Optics EXPRESS

patterns in the two cases are quite similar except the larger scattering in the forward direction for *s*-polarized wave. It implies the close relationship between optical pulling force and directional scattering.

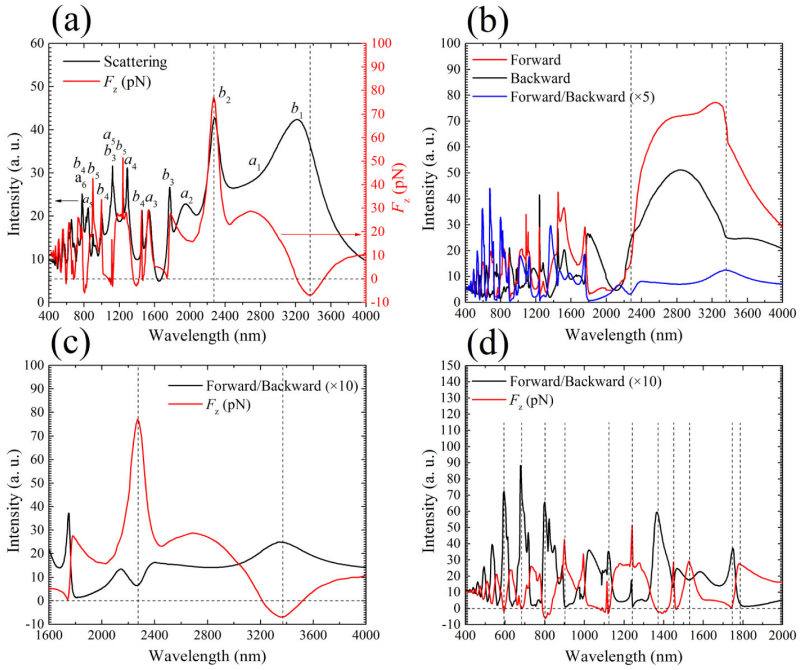

Fig. 7. (a) Wavelength dependence of the optical force in the *z* direction of the Si NS with r = 450 nm calculated for two *s*-polarized waves with θ = 80°. The scattering spectrum of the Si NS calculated by using Mie theory is also provided for comparison. The one-one correspondences between the scattering peaks and the Mie scattering coefficients are indicted in the scattering spectrum. (b) Spectra of the forward and backward scattering and their ratio calculated for the Si NS with r = 450 nm. (c) and (d) show the wavelength dependence of the optical force in the *z* direction and the ratio of the forward to backward scattering in the long- and short-wavelength regions, respectively. The correlations between the maximum optical pulling/pushing force and the maxima/minima of the ratio are indicated by dashed lines.

If we calculated the scattering spectrum of the Si NS with r = 450 nm, it is found that the scattering intensity at λ = 800 nm includes the contributions from the Mie scattering coefficients of a_5, a_6, and b_4, as shown in Fig. 7(a). For the Si NS with r = 450 nm, it is also noticed that optical pulling force is available at other wavelengths such as ~1100 and ~1400 nm [see Fig. 7(a)]. In Fig. 7(b), we show the forward and backward scattering spectra calculated for the Si NS with r = 450 nm which is irradiated by two interfering waves. Also, we present the ratio of the forward to backward scattering in the same figure. In Fig. 7(c), we plot the wavelength dependence of the optical force together with that of the ratio of the forward to backward scattering in the long-wavelength range where the ED, MD, EQ and MQ (corresponding to a_1, b_1, a_2, b_2) are located. It is remarkable that the maximum optical pulling force is achieved at the wavelength of the maximum ratio (λ = 3360 nm) while the maximum optical pushing force is achieved at the wavelength of the minimum ratio (λ = 2270 nm). Similar one-one correspondence can be found in the short wavelength range where high-order electric and magnetic resonances (or high-order Mie scattering coefficients) are located, as shown in Fig. 7(d). However, the minima of optical force do not necessarily mean optical pulling force. On the other hand, it is noticed that the minima of the ratio correspond to the maxima of optical force which is an optical pushing force.

Optics EXPRESS

4. Conclusion

In summary, we have investigated theoretically and numerically the optical pulling and pushing forces acting on Si NSs which possess strong coherent interaction between electric and magnetic resonances. The physical mechanism responsible for the generation of optical pulling force under the irradiation of two interfering waves is elucidated based on the manipulation of the electric and magnetic dipoles induced by the incident light with different polarizations. It was found that optical pulling force with enhanced value and enlarged angle range can be generated for Si NSs whose sizes are much smaller than PS NSs. In addition, very strong optical pushing force is observed at the MQs of Si NSs. It was revealed that the high-order electric and magnetic resonances play a crucial role in generating optical pulling force for Si NSs with large sizes, which is observed not only for *s*-polarized wave but also for *p*-polarized one. The correlation between the optical pulling/pushing force and the directional scattering of Si NSs has been established. While maximum optical pulling force is observed at the maximum of the ratio of the forward to backward scattering, maximum optical pushing force is observed at the minima of the ratio. The engineering and manipulation of optical force will find potential applications in the trapping, transport and sorting of nanoparticles.

Appendix

A.1 Theoretical analysis of the scattering spectra of Si NSs based on the Mie theory

Based on Mie theory, the scattering efficiency Q_{scat} of a single Si NS can be decomposed into a series of multipolar contributions and it can be expressed as [48]:

$$Q_{scat} = \frac{2}{x^2}\sum_{n=1}^{\infty}(2n+1)(|a_n|^2 + |b_n|^2). \tag{4}$$

where $x = kr = 2\pi r/\lambda$, k is the wavevector of light, a_n and b_n denote the electric and magnetic Mie coefficients, λ is the wavelength of light in the ambient medium.

A.2 Optical force generated by two interfering waves

Dipolar particles are usually characterized by their electric and magnetic complex polarizabilities, α_e and α_m, which may be written in the form [43]:

$$\alpha_e = i\frac{3\varepsilon}{2k^3}a_1 \quad \alpha_m = i\frac{3}{2\mu k^3}b_1, \tag{5}$$

Now we consider two plane waves each of which can be characterized by the parameters shown in Fig. 1(b). Here, γ determines the polarization direction in the $\theta_k\phi_k$ plane, θ is the angle between the incident wave and the z axis, ϕ determines the plane of incidence.

A.2.1 Optical force generated by two s-polarized waves

For *s*-polarized wave which is schematically shown in Fig. 1(c), one of the plane waves is characterized by $\gamma_1 = \pi/2, \theta_{k1} = \theta, \varphi_{k1} = 0$ while the other is described by $\gamma_2 = 3\pi/2, \theta_{k2} = \theta, \varphi_{k2} = \pi$. According Eq. (2), we can easily obtain:

$$\vec{k}_1 = (\sin\theta, 0, \cos\theta), \vec{\theta}_1 = (\cos\theta, 0, -\sin\theta), \vec{\phi}_1 = (0, 1, 0), \tag{6}$$

$$\vec{k}_2 = (-\sin\theta, 0, \cos\theta), \vec{\theta}_2 = (-\cos\theta, 0, -\sin\theta), \vec{\phi}_2 = (0, -1, 0). \tag{7}$$

With the help of Eqs. (6) and (7), the electric field of the incident wave can be rewritten as:

Optics EXPRESS

$$\begin{aligned}\vec{E} &= \vec{E}_1 + \vec{E}_2 = E_{1y} + E_{2y} \\ &= E_0(0,1,0)\exp\left[ik\left(x\sin\theta + z\cos\theta\right)\right] + E_0(0,1,0)\exp\left[ik\left(-x\sin\theta + z\cos\theta\right)\right]\end{aligned} \tag{8}$$

In this case, the electric dipole moment is given by:

$$\vec{p} = \vec{p}_1 + \vec{p}_2 = \alpha_e(\vec{E}_1 + \vec{E}_2). \tag{9}$$

Since the light is incident on the *xz* plane, we will consider only the *z* component of the optical force because the *x* and *y* components are much weaker. Because the particle size is very small at the origin of the coordinate, we can choose $x = 0$ so that the complex exponential term can be simplified.

$$\begin{aligned}\left[\left(\nabla\otimes\vec{E}^*\right)\cdot\vec{p}\right]_z &= p_x\nabla_z E_x^* + p_y\nabla_z E_y^* + p_z\nabla_z E_z^* = p_y\nabla_z E_y^* \\ &= -2ik\alpha_e E_0^2\cos\theta - ik\alpha_e E_0^2\cos\theta\exp\left(2ikx\sin\theta\right) \\ &\quad - ik\alpha_e E_0^2\cos\theta\exp\left(-2ikx\sin\theta\right) \\ &= -4ik\alpha_e E_0^2\cos\theta\ (x=0)\end{aligned} \tag{10}$$

Basically, the optical force exerted by the incident wave on the induced electric dipole (i.e. $<F_e>$) can be expressed as [43]:

$$< F_e >_z^s = \frac{1}{2}\Re\left[\left(\nabla\otimes\vec{E}^*\right)\cdot\vec{p}\right]_z = 2kE_0^2\cos\theta\Im(\alpha_e) \tag{11}$$

With the help of Eqs. (6), (7) and (8), we can derive the magnetic fields to be:

$$\vec{B}_1 = \sqrt{\mu\varepsilon}(\vec{k}_1\times\vec{E}_1) = \sqrt{\mu\varepsilon}\left[-\vec{i}E_{1y}\cos\theta + \vec{k}E_{1y}\sin\theta\right] \tag{12}$$

$$\vec{B}_2 = \sqrt{\mu\varepsilon}(\vec{k}_2\times\vec{E}_2) = \sqrt{\mu\varepsilon}\left[-\vec{i}E_{2y}\cos\theta - \vec{k}E_{2y}\sin\theta\right] \tag{13}$$

In this case, the magnetic dipole moment is given by:

$$\vec{m} = \vec{m}_1 + \vec{m}_2 = \alpha_m(\vec{B}_1 + \vec{B}_2) \tag{14}$$

Therefore, the optical force exerted by the incident field on the induced magnetic dipole (i.e. $<F_m>$) is given by:

$$< F_m >_z^s = \frac{1}{2}\Re\left[\left(\nabla\otimes\vec{B}^*\right)\cdot\vec{m}\right]_z = 2k\varepsilon\mu E_0^2\cos^3\theta\Im(\alpha_m) \tag{15}$$

The optical force exerted by the incident field due to the interaction between both dipoles (i.e. $<F_{em}>$):

$$< F_{em} >_z^s = -\frac{k^4}{3}\sqrt{\frac{\mu}{\varepsilon}}\Re\left(\alpha_e\alpha_m^*\right)\left(\vec{E}\times\vec{B}^*\right)_z = -\frac{4\mu k^4}{3}E_0^2\Re\left(\alpha_e\alpha_m^*\right)\cos\theta \tag{16}$$

Previously, the total optical force induced by single plane wave irradiation is expressed as [41]:

$$\left\langle\vec{F}\right\rangle = \left\langle\vec{F}_e\right\rangle + \left\langle\vec{F}_m\right\rangle + \left\langle\vec{F}_{em}\right\rangle = \vec{e}_z\frac{k\varepsilon E_0^2}{2}\left[\Im\left(\varepsilon^{-1}\alpha_e + \mu\alpha_m\right) - \frac{2\mu k^3}{3\varepsilon}\Re\left(\alpha_e\alpha_m^*\right)\right] \tag{17}$$

Optics EXPRESS

If we compare Eqs. (11), (15) and (16) with Eq. (17), it can be easily found that F_e and F_{em} are increased by a factor of $4\cos\theta$ while F_m is increased by a factor of $4\cos^3\theta$ when the illumination of single wave is replaced by the two interfering waves. For this reason, it is expected that F_e and F_{em} decrease at a slower rate ($\cos\theta$) as compared with F_m ($\cos^3\theta$) with increasing θ. As a result, the value of F_{em} may exceed that of F_m and become dominant after a critical value of θ. In this case, a negative force (i.e. pulling force) is generated by the two interfering waves.

A.2.2 Optical force generated by two p-polarized waves

Similar to the *s*-polarized wave, we can use $\gamma_1 = 0, \theta_{k1} = \theta, \phi_{k1} = 0$ and $\gamma_2 = 0, \theta_{k2} = \theta, \phi_{k2} = \pi$ to describe the two *p*-polarized waves schematically shown in Fig. 1(d).

The electric field induced by the two *p*-polarized waves can be written as:

$$\begin{aligned}\vec{E} = \vec{E}_1 + \vec{E}_2 = {} & E_0(\cos\theta, 0, -\sin\theta)\exp[ik(x\sin\theta + z\cos\theta)] \\ & + E_0(-\cos\theta, 0, -\sin\theta)\exp[ik(-x\sin\theta + z\cos\theta)]\end{aligned} \tag{18}$$

So, the optical force acting on the induced electric dipole is given by:

$$< F_e >_z^p = \frac{1}{2}\Re\left[\left(\nabla \otimes \vec{E}^*\right)\cdot\vec{p}\right]_z = 2kE_0^2\cos\theta\sin^2\theta\Im(\alpha_e) \tag{19}$$

Based on Eqs. (6), (7) and (18), the magnetic field can be derived as:

$$\vec{B}_1 = \sqrt{\mu\varepsilon}(\vec{k}_1 \times \vec{E}_1) = \vec{j}\sqrt{\mu\varepsilon}\left(E_{1x}\cos\theta - E_{1z}\sin\theta\right) = B_{1y} \tag{20}$$

$$\vec{B}_2 = \sqrt{\mu\varepsilon}(\vec{k}_2 \times \vec{E}_2) = \vec{j}\sqrt{\mu\varepsilon}\left(E_{2x}\cos\theta + E_{2z}\sin\theta\right) = B_{2y} \tag{21}$$

According to Eqs. (14), (20) and (21), we have

$$< F_m >_z^p = \frac{1}{2}\Re\left[\left(\nabla \otimes \vec{B}^*\right)\cdot\vec{m}\right]_z = \frac{1}{2}\Re\left[m_x\nabla_z B_x^* + m_y\nabla_z B_y^* + m_z\nabla_z B_z^*\right] = 0 \tag{22}$$

With Eq. (18), (20) and (21), we obtain:

$$\begin{aligned}< F_{em} >_z^p &= -\frac{k^4}{3}\sqrt{\frac{\mu}{\varepsilon}}\Re\left(\alpha_e\alpha_m^*\right)\left(\vec{E}\times\vec{B}^*\right)_z \\ &= -\frac{k^4}{3}\sqrt{\frac{\mu}{\varepsilon}}\Re\left(\alpha_e\alpha_m^*\right)\begin{bmatrix}\left(E_{1x}B_{1y}^* - E_{1y}B_{1x}^*\right) + \left(E_{2x}B_{2y}^* - E_{2y}B_{2x}^*\right) \\ + \left(E_{1x}B_{2y}^* - E_{1y}B_{2x}^*\right) + \left(E_{2x}B_{1y}^* - E_{2y}B_{1x}^*\right)\end{bmatrix} \\ &= 0\end{aligned} \tag{23}$$

It is found that the total magnetic dipole disappears for *p*-polarized waves because the two magnetic dipoles induced by the two incident waves are canceled out. Therefore, both F_m and F_{em} equal to zero while F_e remains to be positive. This is why optical pulling force cannot be generated by *p*-polarized waves for small Si NSs. For large Si NSs, the optical force is determined by the high-order electric and magnetic resonances and their coherent interaction.

Funding

National Natural Science Foundation of China (NSFC) (Grant No.11374109 and 11674110); Natural Science Foundation of Guangdong Province, China (Grant No.2016A030308010); Science and Technology Planning Project of Guangdong Province, China (Grant No. 2015B090927006).